

Magnetic Properties of Heavy Ion Implanted Monocrystalline ZnO

J. GOSK^{a,*}, R. PUŻNIAK^b AND A. LYNNYK^b

^a*Faculty of Physics, Warsaw University of Technology,
Koszykowa 75, PL-00662 Warsaw, Poland*

^b*Institute of Physics, Polish Academy of Sciences,
Aleja Lotników 32/46, PL-02668 Warsaw, Poland*

Doi: [10.12693/APhysPolA.141.123](https://doi.org/10.12693/APhysPolA.141.123)

*e-mail: jacek.gosk@pw.edu.pl

Magnetization of monocrystalline ZnO samples implanted with magnetic Co and with Ar and Kr noble gases ions, with energies and doses creating comparable damage, was studied as a function of magnetic field (H) at constant temperature in the temperature range between 2 and 300 K and as a function of temperature for $H = 1$ kOe and 10 kOe. In the Co-implanted ZnO, paramagnetic and some residual ferromagnetic/superparamagnetic phases were revealed, while the Kr- and Ar-implantations do not introduce magnetic centers. The existence of ferromagnetic/superparamagnetic residual phases in the Co-implanted layer was confirmed in the measurements of zero-field cooled/field cooled magnetization at $H = 10, 50,$ and 500 Oe and gave a rise to hysteresis loop appearing in the low temperature range from 2 to 15 K.

topics: ZnO, heavy-ion implantation, magnetic properties

1. Introduction

After two decades of intensive studies on ZnO base diluted magnetic semiconductors (DMSs), still, there is no clear agreement about the nature and origin of the magnetic properties of samples prepared by different methods and by different groups. In particular, this applies to Co ions implanted ZnO. In the literature based both on experimental and theoretical data consideration, the authors point out implantation damages as an origin of magnetic centers in ZnO. On the other hand, there are contradictory opinions shared by the authors of numerous experimental works who did not observe intrinsic ferromagnetic ZnO phase due to different kinds of defects, especially the post-implantation ones [1–6]. In our work [7] it was shown that the defect created in irradiated samples with either electrons or protons prove to be magnetically inactive while those implanted by Co ions reveal the paramagnetic phase (PM). Thus, in the extension of previous studies, the ZnO were implanted with Co and the noble gases Ar and Kr. In order to compare the magnetic properties of ZnO, an attempt was made to establish the implantation conditions causing damage in those samples comparable as regards the range and intensity. Structural studies by means of X-ray and preliminary magnetic properties of Co, Ar, and Kr implanted ZnO were reported in our conference paper [8].

In this research, we report on extended and detailed magnetic studies on Co, Ar, and Kr ions implanted ZnO. Complementary structural investigations of the samples based on Rutherford backscattering and channeling spectroscopy RBS/C were performed by our coworkers and were presented in a separate paper [9]. It has been shown there that Co, Ar, and Kr implanted into ZnO with implemented energies and doses cause comparable damage in the host lattice in terms of its range and magnitude. The thin implanted layers do not reach the amorphization level. Our magnetization measurements revealed, the paramagnetic and some residual ferromagnetic/superparamagnetic phases (FM/SPM) in Co-implanted ZnO and that the Kr- and Ar-implantations do not introduce magnetic centers in ZnO. The existence of FM/SPM residual phases in the Co-implanted layer was confirmed in the measurements of the zero-field cooled/field cooled (ZFC/FC) magnetization.

2. Experiment

The rectangular tiles 5×5 mm², 0.5 mm thick were prepared from commercial Mateck (MaTeck GmbH, Im Langenbroich 20, D-52428 Jülich, Germany) ZnO wurtzite [0001] single crystals (for reference see [10] and [11]). Each studied individual sample constituted two such plates. Two virgin samples of ZnO were implanted with magnetic Co ions

TABLE I

Ions, sample labels, energies, and doses applied in the experiment.

Virgin sample number	Energy [keV]	Fluence $\times 10^{16}$ [cm $^{-2}$]	Total energy $\times 10^{16}$ [keV/cm 2]	Implanted sample name
#1	110	2	220	#1 Φ_{Co}
#5		4	440	#5 $2\Phi_{\text{Co}}$
#2	70	3.14	219.8	#2 Φ_{Ar}
#3		6.3	439.6	#3 $2\Phi_{\text{Ar}}$
#4	160	1.37	219.2	#4 Φ_{Kr}
#6		2.75	438.4	#6 $2\Phi_{\text{Kr}}$

of 110 keV energy and with two fluences of $2 \times 10^{16}/\text{cm}^2$ and $4 \times 10^{16}/\text{cm}^2$. The energies of Ar and Kr ions producing equivalent/appropriate damage ranges, i.e., identical with that related to 110 keV Co in ZnO and to two studied fluences were given in our previous work [8]. Base on these preliminary energy and dose considerations four virgin samples of ZnO were implanted with the appropriate energy and fluences of Ar and Kr ions as presented in Table I. No thermal annealing has been performed for the studied samples since it was shown already that the damage produced by implantation does not reach an amorphization level [9]. The ballistic nature of the implantation process was observed in the aligned spectra for ZnO implanted samples as a characteristic damage peak reaching a depth of 200 nm in the case of Co and Kr implantation and 140 nm for Ar ions (for more details see [9]).

Samples for magnetic measurements were mounted in the way described in our previous work [8]. Magnetization was measured using a superconducting quantum interference device SQUID MPMS XL magnetometer. Magnetic field was applied in the geometry parallel to the surface of the sample. For complete magnetic characterization of the Co, Kr, and Ar implanted ZnO, all samples undergo the following measurement procedure:

1. magnetization was measured as a function of magnetic field (M vs H) in the range from 0 to 60 kOe at different temperatures ($T = 2, 5, 20, 50, 100, 200,$ and 300 K),
2. magnetization was measured as a function of temperature (M vs T) at $H = 1$ kOe and $H = 10$ kOe in the temperature range from 2 to 300 K.

To investigate ferromagnetic/superparamagnetic (FM/SPM) residual phases in the Co-implanted layer, the zero-field cooled/field cooled magnetization was recorded at $H = 10, 50,$ and 500 Oe. For the Co-implanted ZnO, hysteresis loops M - H at $T = 2.0, 3.5, 5.0, 7.5, 10.0, 12.5, 15.0$ K in the magnetic field range from -60 kOe to 60 kOe were measured.

3. Results and discussion

3.1. $M(T)$ and $M(H)$ measurements

We start the data analysis by presenting the M vs T data at $H = 10$ kOe. The collected experimental curves for all groups of virgin/parent ZnO (notation #1-#6) and the relevant Co-, Ar-, and Kr-implanted ZnO samples are shown in Fig. 1.

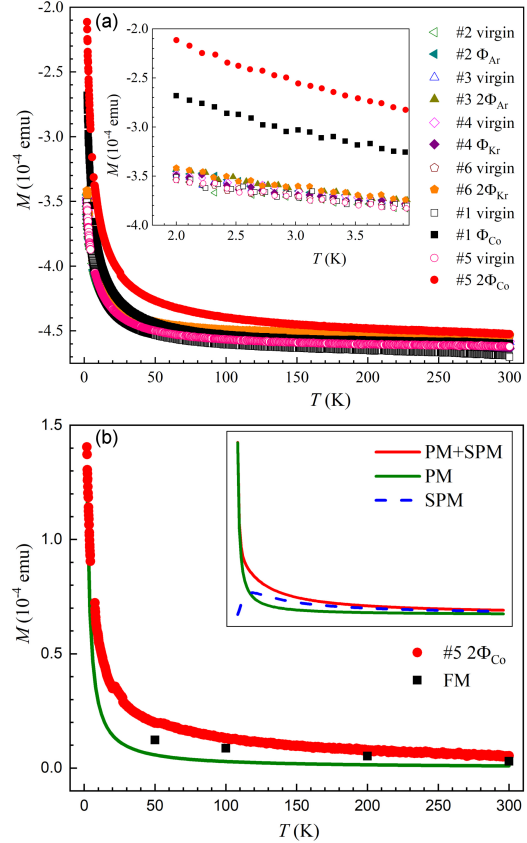


Fig. 1. (a) The dependence M vs T for six virgin ZnO and relevant Co, Ar, and Kr ion-implanted ZnO, measured at $H = 10$ kOe. The same data in low temperature range, i.e., from 2 to 4 K is presented in the inset. (b) M vs T at 10 kOe for ZnO #5 $2\Phi_{\text{Co}}$ sample after correction for parent ($M_{\text{vir, tot}}$) signal of ZnO (#5). Thin green line represents PM_{impl} curve calculated using the Brillouin function with parameters obtained by fitting paramagnetic $M(T)$ dependence to M vs H data collected at 2 K (corrected for virgin signal and for $M_{\text{FM/SPM, impl}}$; see procedure described in the text). The black squares are experimental points taken (for $H = 10$ kOe) from the dependence M vs H measured at 50, 100, 200, and 300 K. In the inset, it is shown schematically how the total magnetization coming from a thin implanted layer (TIL) could be decomposed at a low magnetic field on PM_{impl} and $\text{FM/SPM}_{\text{impl}}$ contributions. It will be discussed in details further in the description of Fig. 3.

For convenience, to track the analysis of magnetization data, all components of the total magnetization $M_{\text{impl, tot}}$ that were measured for the implanted samples, were enumerated as follows

$$M_{\text{impl, tot}} = M_{\text{dia}_{\text{int}}} + M_{\text{PM}_{\text{int}}} + M_{\text{PM}_{\text{impl}}} + M_{\text{FM/SPM}_{\text{impl}}} + M_{\text{dia}_{\text{glu, impl}}}, \quad (1)$$

where the first and second components on the right-hand side in (1) are diamagnetic $M_{\text{dia}_{\text{int}}}$ and paramagnetic $M_{\text{PM}_{\text{int}}}$ contributions pertaining to the virgin sample ZnO, respectively, while the third and fourth are those originating from the paramagnetic PM_{impl} and residual $\text{FM/SPM}_{\text{impl}}$ phases, respectively, present in the thin implanted layer. The last component in (1) is the diamagnetic signal from the glue. Generally, contributions pertaining to PM_{impl} and residual $\text{FM/SPM}_{\text{impl}}$ could be recovered due to the correction procedure. Note that total magnetization $M_{\text{vir, tot}}$ of the virgin sample has the following contributions

$$M_{\text{vir, tot}} = M_{\text{dia}_{\text{int}}} + M_{\text{PM}_{\text{int}}} + M_{\text{dia}_{\text{glu}}}. \quad (2)$$

Thus, in principle

$$M_{\text{impl, tot}} - M_{\text{vir, tot}} = M_{\text{PM}_{\text{impl}}} + M_{\text{FM/SPM}_{\text{impl}}} + (M_{\text{dia}_{\text{glu, impl}}} - M_{\text{dia}_{\text{glu}}}) \cong M_{\text{PM}_{\text{impl}}} + M_{\text{FM/SPM}_{\text{impl}}}. \quad (3)$$

It should be noted that to minimize the error introduced by the subtraction procedure, the sample before and after implantation should be stuck ideally in the same position in the diamagnetic straw used during the measurements.

Since the sample masses are only slightly different among the measured samples (136.61–140.27 mg), the magnetization curves (Fig. 1a) of all six virgin ZnO samples (#1–#6) should practically overlap, and indeed it is observed. In general, the total magnetization for both implanted and not-implanted ZnO groups ($M_{\text{impl, tot}}$ and $M_{\text{vir, tot}}$) is dominated by diamagnetic contributions $M_{\text{dia}_{\text{int}}}$ of ZnO lattice accompanied by a weaker paramagnetic $M_{\text{PM}} = M_{\text{PM}_{\text{int}}} + M_{\text{PM}_{\text{impl}}}$. Both contributions, M_{PM} and $M_{\text{dia}_{\text{int}}}$, could be clearly monitored due to their different magnetic behavior. The magnetization dependences of all samples in the temperature range from about 100 to 300 K slightly decreased with increasing temperature and became almost constant amounting of about 4.6×10^{-4} emu at 300 K. Thus, the magnetic susceptibility $\chi_0 \cong 3.36 \times 10^{-7}$ emu/(Oe g), estimated from the high temperatures range, is in accord with the literature data for ZnO. All experimental curves almost overlap at high temperatures, where the diamagnetic contribution prevails. Due to Curie law, the PM contribution of magnetic impurities ($M_{\text{PM}_{\text{int}}}$) from parent ZnO is readily seen at low temperatures $T \leq 20$ K. This is shown in the inset of Fig. 1a. The first important observation is that magnetization curves for Ar or Kr ion-implanted ZnO, namely #2 Φ_{Ar} , #3 $2\Phi_{\text{Ar}}$, #4 Φ_{Kr} , and #6 $2\Phi_{\text{Kr}}$, overlap

with those of the virgin samples. An additional magnetic contribution is present in the Co-implanted ZnO (samples #1 Φ_{Co} and #5 $2\Phi_{\text{Co}}$) in M vs T curves, contrary to that of Ar and Kr ion-implanted ZnO (see inset in Fig. 1a). In accord with our previous investigation [7], the additional PM contribution ($M_{\text{PM}_{\text{impl}}}$) coming from Co ion-implanted ZnO layers is well distinguished. Secondly, one can observe that when the fluence of the Co ions increases from 2×10^{16} cm $^{-2}$ to 4×10^{16} cm $^{-2}$, the PM_{impl} contribution increases by a factor of ~ 1.5 . Moreover, the comparison of the magnetization curves of virgin ZnO with the Co ions implanted ZnO (samples #5 $2\Phi_{\text{Co}}$ — closed red circles) in the high temperature range suggests the presence of some additional residual phase/phases. It is clearly visible for $T > 40$ K, where the total PM contribution strongly weakens according to Curie law. To investigate this case more precisely, the magnetization of Co ions implanted ZnO were corrected for the magnetization of parent ZnO. However, one should keep in mind (see the text above) that small differences in the sample mounting can result in a change of few percent of the $M_{\text{impl, tot}} - M_{\text{vir, tot}}$. The resultant curve obtained due to subtraction procedure ($M_{\text{impl, tot}} - M_{\text{vir, tot}}$) would be affected by erroneous component. Figure 1b shows M vs T at $H = 10$ kOe after correction procedure, thus presenting $M_{\text{PM}_{\text{impl}}} + M_{\text{FM/SPM}_{\text{impl}}}$ signal alone originating from thin implanted layer (TIL) of #5 $2\Phi_{\text{Co}}$ — the sample with higher Co ions fluence of 4×10^{16} cm $^{-2}$. The presence of two magnetic phases in the investigated layer is clearly manifested in Fig. 1b, i.e., PM_{impl} dominating at low temperatures and $\text{FM/SPM}_{\text{impl}}$ dominating at $T > 20$ K [12, 13]. However, it should be stressed that the decomposition of the total magnetization into two/three contributions cannot be done accurately without additional information about the PM and FM/SPM phases.

The presence of two phases in Co implanted TIL (samples #1 Φ_{Co} and #5 $2\Phi_{\text{Co}}$) can be inferred from the M vs H dependence at $T = 2, 5, 10, 20, 50, 100, 200, 300$ K. The relationships of the M vs H curves of #1 Φ_{Co} and #5 $2\Phi_{\text{Co}}$ samples after the correction for magnetization of the parent virgin sample are depicted, respectively, in Fig. 2a and b.

Generally, the magnetization curves (Fig. 2a and b) show a typical PM behavior. At low temperatures (e.g. 2 K), the magnetization reveals a pronounced tendency to saturate with increasing magnetic field, while at high temperatures ($T > 50$ K) the magnetization is practically a linear function of the magnetic field. The residual phase manifests itself by a rapid increase of magnetization at a low magnetic field ($H \leq 15$ kOe). The magnetization of additional phase could be obtained for $T \geq 50$ K by subtracting the linear PM_{impl} contribution from the $M_{\text{PM}_{\text{impl}}} + M_{\text{FM/SPM}_{\text{impl}}}$. The results of this procedure are shown in Fig. 2c and 2d.

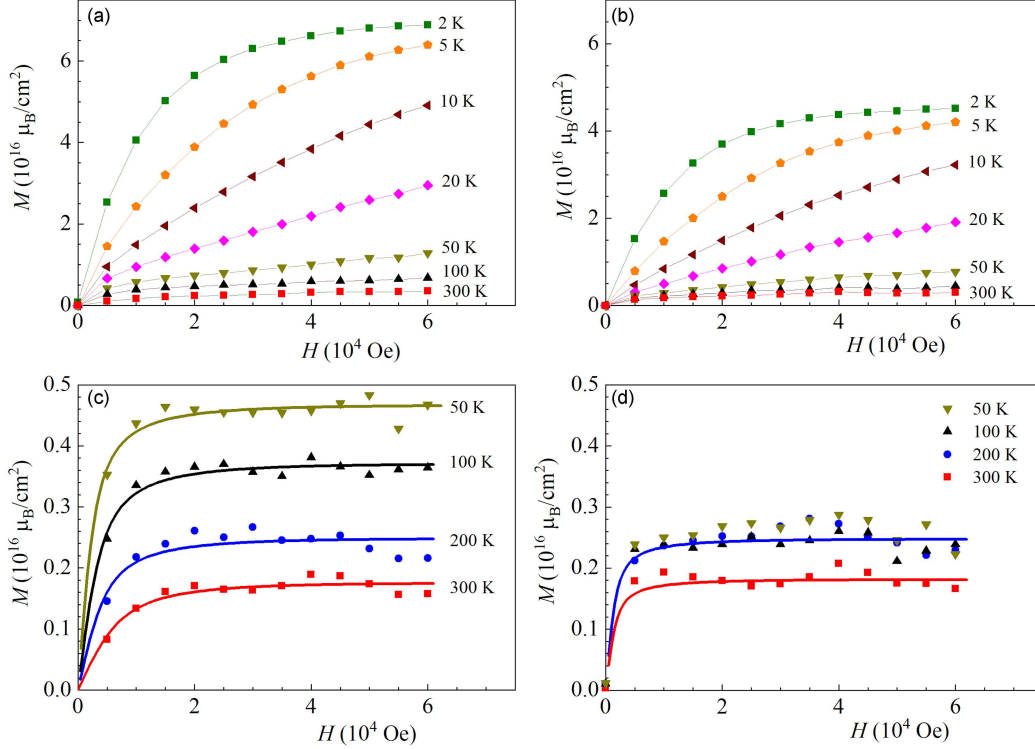


Fig. 2. The dependence M vs H for different temperatures after correction for virgin signal (see (3)) for sample #5 $2\Phi_{\text{Co}}$ (a) and for sample #1 Φ_{Co} (b). Lower panels represent residual contribution $M_{\text{FM/SPM}_{\text{impl}}}$ from TIL obtained following to correction procedure (see the text) for sample #5 $2\Phi_{\text{Co}}$ (c) and for sample #1 Φ_{Co} (d). Note different scales on the M -axes in upper and lower panels.

The experimental curves (Fig. 2c and d) are characterized by a rapid increase of magnetization at a low magnetic field and saturation in higher magnetic fields. This observation, together with those coming from M vs T measurements, suggests the presence of some residual FM/SPM_{impl} phase in the implanted layer. However, one should note the difference between the two samples. The FM/SPM_{impl} magnetization of #1 Φ_{Co} sample starts to be saturated at $H \cong 5$ kOe and its value $M_{\text{sat}} \cong 2.4 \times 10^{16} \mu_{\text{B}}/\text{cm}^2$ does not depend on the temperature in the temperature range from 50 to ~ 200 K and slightly decreases when rising to 300 K. Note that M vs H curves at $T = 300$ and 200 K exhibit almost the same M_{sat} values for the #1 Φ_{Co} and #5 $2\Phi_{\text{Co}}$ samples, but they are starting to saturate at a higher magnetic field $H \cong 15$ kOe in the case of #5 $2\Phi_{\text{Co}}$ sample. What is more, in accord with the already presented dependence M vs T at $H = 10$ kOe (Fig. 1a), lowering the temperature from 200 to 100 K and further to 50 K causes a monotonic increase of M_{sat} . These experimental facts indicate that a double increase of fluence results in an appearing additional contribution in the total residual FM/SPM_{impl} magnetic response. It will be shown further that this additional magnetic contribution could be attributed to the appearance of SPM clusters with a low blocking temperature T_B .

It should be recalled that clusters of few ferromagnetically coupled Co ions as well as nanoparticles of antiferromagnetic CoO, Co₃O₄, and Co₂O₄ and ferromagnetic ZnCo₂O₄ (observed as a secondary phase in Co-doped ZnO [12], and literature cited therein) should behave as nanoparticles with high magnetic moment (a few μ_{B}), i.e., as superparamagnetic particles SPM [13]. However, in the work of Banerjee et al. [14], ferromagnetism in ZnO, attributed to formation of oxygen vacancy clusters with T_B above 340°C, and thus formation of the FM/SPM phase in ZnO without the presence of magnetic ions, was reported.

To characterize further magnetic properties of both phases, i.e., PM_{impl} and FM/SPM_{impl}, we made some rough estimate. Since at $T < 50$ K the dependence M vs H dependence of paramagnetic phase stops being linear, thus the total signal cannot be precisely decomposed into PM and FM/SPM_{impl} phases. Nevertheless, we assumed that M vs H for an additional FM/SPM contribution at $T = 50$ K approximates the M vs H curves quite well for $M_{\text{FM/SPM}_{\text{impl}}}$ at lower temperatures. The M vs H of #5 $2\Phi_{\text{Co}}$, corrected in this way for the data collected at $T = 2$ K, was well approximated by the Brillouin function with spin $S = 2$. However, because of the way we obtained this result, we can only infer that the value of S is roughly equal to 2. Comparing our measurement

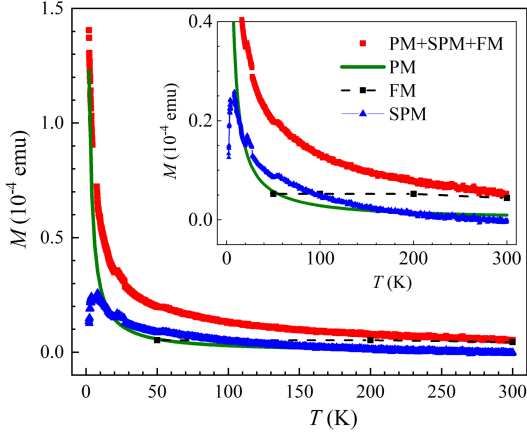


Fig. 3. M vs T for TIL of #5 $2\Phi_{\text{Co}}$ sample — red squares. Thin green line represents PM_{impl} , calculated using the Brillouin function (see Fig. 1b). Black points represent the FM obtained from M vs H curves (see Fig. 2d). The same curves for $0 \leq M \leq 0.4 \times 10^{-4}$ emu are shown on the extended scale in the inset.

data with the results from the work of Wojnarowicz et al. [12] in which the magnetization of $\text{Zn}_{1-x}\text{Co}_x\text{O}$ for $0.01 \leq x \leq 0.15$ was measured, we can state that in our TIL for $x \leq 0.01$, practically the entire volume of TIL is paramagnetic.

A summary of described above magnetic data is presented in Fig. 3, which shows the dependence M vs T for the #5 $2\Phi_{\text{Co}}$ sample and its components, i.e., PM_{impl} , FM_{impl} , and SPM_{impl} phases.

The curves representing the PM and FM phases were obtained based on the measurements of the M vs H dependences. The $M_{\text{SPM}_{\text{impl}}}$ curve was obtained from the measured temperature dependence of magnetization $M_{\text{PM}_{\text{impl}}} + M_{\text{FM}/\text{SPM}_{\text{impl}}}$ of #5 $2\Phi_{\text{Co}}$ sample after subtracting both $M_{\text{PM}_{\text{impl}}}$ and $M_{\text{FM}_{\text{impl}}}$ curves. We assume that FM_{impl} is roughly equal for both #1 Φ_{Co} and #5 $2\Phi_{\text{Co}}$ samples. The values of $M_{\text{PM}_{\text{impl}}}$ were calculated using the Brillouin function as already described (vid infra). To confirm the validity of this qualitative picture of the magnetic properties of the #5 $2\Phi_{\text{Co}}$ sample, further measurements presented in Sect. 3.2, were performed.

3.2. Zero-field cooled/field cooled (ZFC/FC) measurements and hysteresis

The properties of $\text{FM}/\text{SPM}_{\text{impl}}$ phase were studied by measuring zero-field cooled/field cooled (ZFC/FC) temperature dependence recorded at $H = 10, 50,$ and 500 Oe shown in Fig. 4. One should keep in mind that $M_{\text{FM}/\text{SPM}_{\text{impl}}}$ is the minor contribution in $M_{\text{impl, tot}} = M_{\text{PM}_{\text{impl}}} + M_{\text{FM}/\text{SPM}_{\text{impl}}}$.

It is readily seen in Fig. 4 that, the ZFC and FC curves do not overlap at low temperatures. On the FC curves measured at $H = 10$ Oe and at $H = 50$ Oe, blocking temperature $T_B \cong 4.2$ K

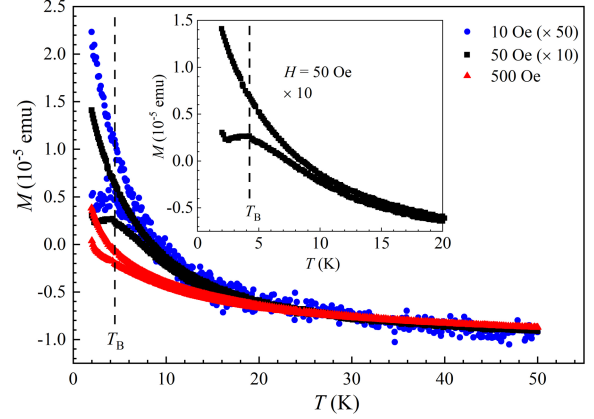


Fig. 4. The ZFC–FC magnetizations of #5 $2\Phi_{\text{Co}}$ sample at $H = 10$ Oe — blue circles, $H = 50$ Oe — black squares, and $H = 500$ Oe — red triangles. Magnetization values of curves measured at $H = 10$ Oe and $H = 50$ Oe are multiplied by 50 and 10, respectively. The inset shows ZFC–FC measured at $H = 50$ Oe in the temperature range from 2 to 20 K.

(the maximum on ZFC curve), typical for superparamagnetic particles, is well discernible. Characteristically, the distance between ZFC and FC curves clearly decreases as the field H increases. Furthermore, for the strongest $H = 500$ Oe, the maximum practically vanishes. For $T \gg T_B$, ZFC and FC of SPM should overlap and be H/T dependent. Thus, the six curves were properly normalized (the magnetization measured at $H = 10$ Oe and at $H = 50$ Oe were multiplied by 50 and 10, respectively). Indeed, the normalized magnetization dependences, collected at three different H , practically overlap at the highest observed temperatures. However, from the magnetization of ZFC and FC at $H = 50$ Oe (signal not very noisily, and thus measurements performed at a sufficiently low $H = 50$ Oe), it is seen that at much higher temperature the ZFC curve still departs from the corresponding ZFC and starts to overlap for temperatures higher than about 40 K.

Non-disappearing hysteresis loop could be observed in the temperature range in which the ZFC/FC curves do not overlap. The hysteresis loops of M – H were measured for $T = 2.0, 3.5, 5.0, 7.5, 10.0, 12.5,$ and 15.0 K. The two selected examples of raw data are presented in Fig. 5.

To observe the change of the saturation remanence M_r and coercivity of remanence H_{cr} as a function of temperature, the curves obtained by subtracting the ascending curve (-60 kOe \rightarrow 60 kOe) from the descending one (60 kOe \rightarrow -60 kOe), i.e., ΔM vs H , were analyzed (see Fig. 6a).

We recall that the saturation remanence is defined as the magnetization remaining in the zero applied field after decreasing from the saturation

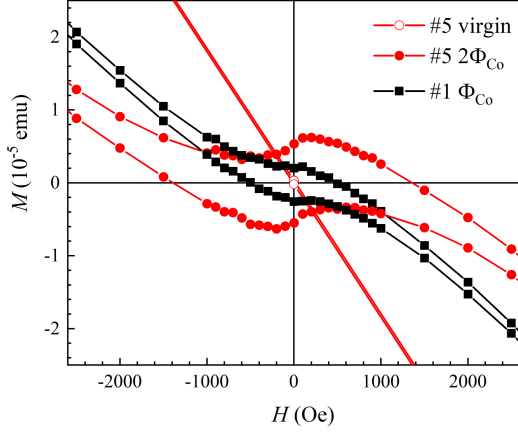


Fig. 5. Row magnetization data for M - H hysteresis loop at $T = 2$ K for #1 Φ_{Co} and for #5 $2\Phi_{\text{Co}}$ samples (not corrected for diamagnetic and for PM background). For comparison reference M - H curve of virgin material of #5 (virgin sample), measured at $T = 2$ K, is added.

magnetization, and therefore the maximum on the curve in Fig. 6a is equal to $2M_r$. The coercivity of remanence is defined as the magnetic field required to irreversibly flip half of the magnetic moments in the SPM particles. The two values M_r and H_{cr} can be read from the curve in Fig. 6a (at $H = H_{cr}$ the curve assumes a value equal to $0.5 \times \Delta M_{\text{max}}$). A rapid disappearance of the hysteresis loops is suggested for $T > T_B$ and this is actually seen for temperatures above $T_B \approx 4.2$ K, as determined from the ZFC curves (see, Fig. 6b and Fig. 4). However, some small background, decreasing very slowly with increasing H , is observed in both #1 Φ_{Co} and #5 $2\Phi_{\text{Co}}$ samples and correlates well with non-overlapping of ZFC and FC curves (see, Fig. 6b and Fig. 4). The experimental data of this and the previous paragraphs allow to draw the following conclusion. The total residual magnetization of TIL pre-mark as FM/SPM_{impl} consists of two contribution, i.e., one with T_B slightly higher than room temperature and the other with a low temperature $T_B \approx 4.2$ K. The first one is observed in the almost same amount, in both Co implanted samples, while the one with low $T_B \approx 4.2$ K is mainly present in the #5 $2\Phi_{\text{Co}}$ sample.

Generally, magnetization of #5 $2\Phi_{\text{Co}}$ sample scales very well with that of #1 Φ_{Co} . In particular, the M vs H curves measured for $T = \text{const}$, representing (after correction procedure) PM_{impl} of #1 Φ_{Co} , coincide, when multiplied by a common factor, with the relevant curves of the #5 $2\Phi_{\text{Co}}$ sample. However, a two-fold increase of Co ions fluence results in lower then proportional increase of magnetization. We observed $M(6 \text{ T}) = 4.2 \times 10^{16} \mu_{\text{B}}/\text{cm}^2$ for #1 Φ_{Co} sample implanted with fluence $2 \times 10^{16} \text{ cm}^{-2}$ while $M(6 \text{ T}) = 6.8 \times 10^{16} \mu_{\text{B}}/\text{cm}^2$ for #5 $2\Phi_{\text{Co}}$

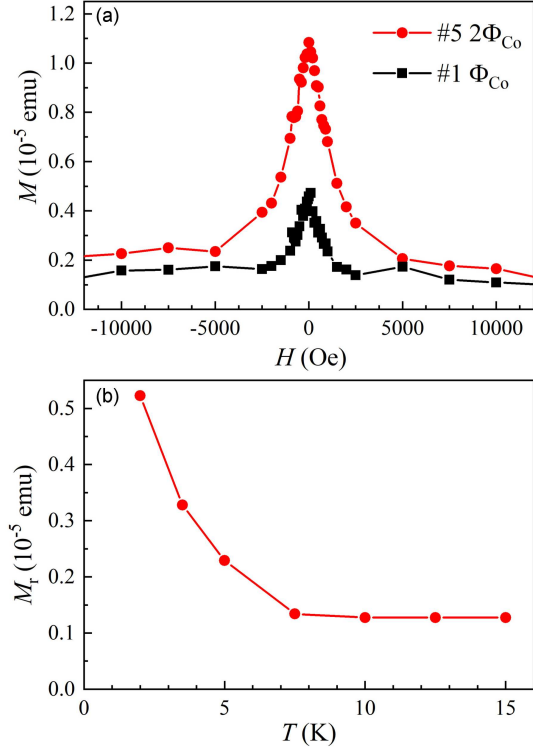


Fig. 6. Co-implanted ZnO samples: #5 $2\Phi_{\text{Co}}$ — closed red circles, #1 Φ_{Co} — black squares. (a) The dependence ΔM vs H at 2 K, i.e., the curve obtained by subtracting the ascending curve of M - H loop (magnetic field increasing from -60 kOe to 60 kOe) from the descending one (H decreasing from 60 kOe to -60 kOe). (b) Saturation remanence M_r dependence on temperature for #5 $2\Phi_{\text{Co}}$ sample.

sample implanted with fluence $4 \times 10^{16} \text{ cm}^{-2}$, with both PM_{impl} and FM/SPM_{impl} phases practically saturated at $H = 6$ kOe. Hence, it is easy to see that the magnetic moment per Co atom (μ_{B}/Co) amounts to about 2.1 in the case of the sample with Co dose of $2 \times 10^{16} \text{ cm}^{-2}$ and to about 1.7 in the case of the sample with Co dose of $4 \times 10^{16} \text{ cm}^{-2}$. On the other hand, the total residual $M_{\text{FM/SPM}_{\text{impl}}}$ contribution of #5 $2\Phi_{\text{Co}}$ is more than twice higher than that of #1 Φ_{Co} sample. What is more, experimental data revealed that in the total FM/SPM_{impl} the same amount of the high $T_B > 300$ K contribution is observed in both samples, while low $T_B \approx 4.2$ K contribution is much more abundant in #5 $2\Phi_{\text{Co}}$ sample.

4. Conclusions

All investigated Co, Ar, and Kr ions implanted ZnO do not reveal intrinsic/bulk FM. The paramagnetic phase was observed in Co ions implanted ZnO, as was reported in our previous work. It could be well explained by the weakly interacting Co ions, partly substituting Zn ions and partly at interstitial

positions. In addition, the same residual superparamagnetic/ferromagnetic phase was observed, most likely derived from small Co ion clusters. No change in magnetic properties was observed in ZnO implanted with Ar and Kr ions. Assuming a similar nature of defects generated by Co and Ar and Kr ions, we conclude that the defects resulting from implantation in the examined energy and intensity range for magnetic Co ions, as well as non-magnetic Ar and Kr, are not magnetically active.

References

- [1] S. Mal, S. Nori, J. Narayan, J.T. Prater, D.K. Avasthi, *Acta Mater.* **61**, 2763 (2013).
- [2] A.S. Fedorov, M.A. Visotina, A.S. Kholtochina, A.A. Kuzubov, N.S. Mikhaleva, HuaShu Hsu, *J. Magn. Magn. Matter.* **440**, 5 (2017).
- [3] L.M.C. Pereira, J.P. Araújo, U. Wahl, S. Decoster, M.J. Van Bael, K. Temst, A. Vantomme, *J. Appl. Phys.* **113**, 023903 (2013).
- [4] J.J. Lee, G.Z. Xing, J.B. Yi, T. Chen, M. Ionescu, S. Li, *Appl. Phys. Lett.* **104**, 012405 (2014).
- [5] Yubin Huang, Wei Zhou, Ping Wu, *Sol. State Commun.* **183**, 31 (2014).
- [6] M. Xu, H. Yuan, B. You, P.F. Zhou, C.J. Dong, M.Y. Duan, *J. Appl. Phys.* **115**, 093503 (2014).
- [7] Z. Werner, J. Gosk, A. Twardowski, M. Barlak, C. Pochrybniak, *Nucl. Instrum. Meth. Phys. Res. B* **358**, 174 (2015).
- [8] J.B. Gosk, Z. Werner, G. Kowalski, M. Tokarczyk, R. Puźniak, M. Barlak, *Acta Phys. Pol. A* **136**, 628 (2019).
- [9] Z. Werner, M. Barlak, R. Ratajczak, S. Akhmadaliev, R. Heller, B. Staszkiwicz, J. Zagórski, *Radiat. Eff. Defects in Solids* **176**, 538 (2021).
- [10] MaTecK, *Introduction Crystals and Crystal Growth*.
- [11] MaTeK, *ZnO, Zinc oxide*.
- [12] J. Wojnarowicz, M. Omelchenko, J. Szczytko, T. Chudoba, S. Gierlotka, A. Majhofer, A. Twardowski, W. Lojkowski, *Crystals* **8**, 410 (2018).
- [13] M. Woińska, J. Szczytko, A. Majhofer, J. Gosk, K. Działkowski, A. Twardowski, *Phys. Rev. B* **88**, 144421 (2013).
- [14] S. Banerjee, M. Mandal, M. Gayathri, M. Sardar, *Appl. Phys. Lett.* **91**, 182501 (2007).